Indian Journal of Pure & Applied Physics
Vol. 64, September 2026, pp. 1029-1038
DOI: 10.56042/ijpap.v64i9.31143

# Optimized Hollow-Core Photonic Crystal Fiber Based Gas Sensor

Md Tahseen Alam & Sandhir Kumar Singh*

Department of science, Indian Institute of Information Technology Ranchi, Jharkhand 835 217, India

*Received: 7th May 2026; accepted: 7th July 2026*

This paper proposes the design of a rigorously optimized hollow-core photonic crystal fiber (HC-PCF) gas sensor for sensitive detection of methane ($CH_4$) at the 1.67μm near infrared absorption line. A complete vector finite element method (FEM) within COMSOL Multiphysics and a Python-based numerical method employing an Anti-Resonant Reflecting Optical Waveguide (ARROW) model were used with perfectly matched layer (PML) boundary conditions to assess the modal attributes, confinement loss, and gas sensing features of the proposed fiber. The central hollow-core diameter, cladding air-hole diameter, and hole pitch are essential geometric parameters, which have been optimized to enhance the interaction of the guided fundamental mode's evanescent field with the target analyte gas in the hollow core. The optimization demonstrates that this HC-PCF exhibits a relative sensitivity of about 97% with a confinement loss of 0.007dB/m at 1.67μm. In addition to conventional sensitivity and loss characterization, the paper provides three analyses that have, to the best of authors' knowledge, not been previously reported for this class of sensor: (i) curvature loss characterization for bend radius of 5–20 mm; (ii) temperature dependent sensitivity analysis over −20 °C to 80°C; and (iii) fabrication tolerance assessment quantifying effect on sensing performance of ±5 % deviations from manufacture of core diameter, pitch and hole diameter. Moreover, the effective refractive index, numerical aperture, V-parameter, and power fraction were retrieved to ensure that stable single-mode guidance occurs in the sensing region. The high sensitivity plus low propagation losses, good tolerance to the ambient environment, and ease of fabrication of this design make it a serious contender for methane detection for environmental monitoring and industrial safety applications.

**Keywords:** Hollow-core photonic crystal fiber, Gas sensor, Finite element method, Confinement loss, Relative sensitivity, Bending loss, Fabrication tolerance, Temperature stability, Methane detection

## 1 Introduction

Fiber-optic communication systems serve as the backbone of modern global telecommunication[1,2]. Apart from telecommunication, optical fibres have also found extensive applications for sensing applications due to their inherent immunity to electromagnetic interference, electrical isolation as well as capability of remote operation. The ordinary step-index fibers restrict the tunability of their optical features which has resulted in the development of photonic crystal fibers (PCFs) with enhanced features. These micro-structured optical fibers allow extraordinary tunability with small geometric changes[3,4]. PCFs consist of a silica matrix perforated by a periodic array of air holes running along the fiber axis[4]. The hollow-core variant is particularly attractive for gas sensing because the direct overlap between the guided optical mode and the gas filling the hollow core yields substantially higher sensitivity compared with solid-core designs, in which light interacts only weakly with analyte molecules residing in the cladding[5,6].

*Corresponding author: E-mail: sksingh@iiitranchi.ac.in

PCFs offer a compelling combination of properties for sensing, including high birefringence, enhanced optical nonlinearity, single-mode or few-mode operation, engineerable chromatic dispersion, and low bending and splice losses[4,7]. Their capability to function as gas or liquid sensors upon filling the air holes with analytes makes them exceptionally versatile[5,6]. Gas sensing is of paramount importance across a broad range of applications, including environmental pollution monitoring, industrial process control, pharmaceutical and petrochemical facility safety, and protection of high-voltage electrical substations[8,9,10] . PCF-based gas sensors offer compelling operational advantages over conventional electrochemical sensors: immunity to electromagnetic interference, the absence of electrical conductivity in the sensing element, safe operation in corrosive or explosive atmospheres, and suitability for long-range remote monitoring[8,11].

While both solid-core and hollow-core PCF architectures have been employed for gas sensing, their underlying mechanisms and achievable sensitivities differ substantially[11,12]. Solid-core PCFs exhibit inherently limited sensitivity because light-gas interaction is restricted to the evanescent field extending into the cladding air holes[13,14]. Hollow-core PCFs overcome this fundamental limitation by guiding light predominantly within the hollow core via the photonic bandgap effect, enabling direct and substantial light-gas interaction[6,15-17].

Nevertheless, prior work on HC-PCF gas sensors has suffered from one or more significant limitations. First, a high sensitivity of 99.98 % at 1.56 μm was reported[17], but at the cost of an excessively high confinement loss of approximately 20dB/m, which severely constrains usable fiber length and detection precision. Second, numerous studies report limited sensitivity achieved only 27.58 % at 1.33 μm, and 41 % at 1.53 μm was reported[18,19]. Third, and most critically, the majority of prior works[19-24] have focused exclusively on sensitivity and confinement loss, neglecting practical deployment factors such as bending loss, thermal stability, and fabrication tolerance all of which are essential for reliable field operation.

In order to address these challenges, the present work provides a design of HC-PCF with high sensitivity and ultra-low confinement loss. In this work, a step-by-step optimized HC-PCF gas sensor for methane detection, based on high relative sensitivity, and ultra-low confinement loss is presented. In addition to the conventional characterization of sensitivity and propagation loss, this study systematically investigates three practically relevant performance metrics bending loss, temperature stability, and fabrication tolerance which, to the best of authors' knowledge, have not yet been reported in the literature for this class of sensors.

## 2 Governing Equations

The principal optical characteristics of a PCF-based gas sensor are the confinement loss and relative sensitivity[11,12]. The confinement loss is related to the imaginary part of the effective complex mode index and is evaluated as[12,24];

$$L_c = 8.686 K_0 \mathrm{Im}[n_{eff}] \text{ [dB/m]} \quad \text{... (1)}$$

where $L_c$ is the confinement loss, $\mathrm{Im}[n_{eff}]$ is the imaginary component of the complex effective refractive index, and $K_0 = 2\pi/\lambda$ is the free-space wavenumber.

The transmitted gas concentration is derived from the detected optical power using the Beer–Lambert law[11,16];

$$I(\lambda) = I_0(\lambda)\exp[-r\theta_m(\lambda)LC] \quad \text{... (2)}$$

where $I(\lambda)$ is the output intensity in the presence of gas, $I_0(\lambda)$ is the reference intensity in the absence of gas, $\alpha_m(\lambda)$ is the wavelength-dependent molecular absorption coefficient of the analyte, L is the interaction length, C is the gas concentration, and r is the relative sensitivity coefficient.

The relative sensitivity is given by[12,22];

$$r = \frac{n_r}{n_{eff}} f \quad \text{... (3)}$$

where $n_r$ is the refractive index of the analyte gas and f is the fractional optical power confined within the gas-filled hollow core;

$$f = \frac{\int_{hole}(E_x H_y - E_y H_x)dxdy}{\int_{total}(E_x H_y - E_y H_x)dxdy} \quad \text{... (4)}$$

where $E_x$, $E_y$ and $H_x$, $H_y$ denote the transverse electric and magnetic field components of the guided mode, respectively[6,24].

The macro bending loss for the fundamental mode is estimated using the adapted Marcuse formula[3,7,24];

$$\alpha_{bend} = \frac{\sqrt{\pi}}{2\gamma^{3/2} a \sqrt{R}} \exp\left(-\frac{2\gamma^3 R}{3 k_0^2 n_{eff^2}}\right) \quad \text{... (5)}$$

where $\gamma$ is the field decay constant in the cladding, a is the core radius, and R is the bending radius.

The refractive index dispersion of fused silica is modeled using the three-term Sellmeier equation[25];

$$n^2(\lambda) = 1 + \sum_{i=1}^{3} \frac{B_i \lambda^2}{\lambda^2 - C_i} \quad \text{... (6)}$$

with coefficients $B_1 = 0.6962$, $C_1 = 0.00468 \mu m^2$; $B_2 = 0.4079$, $C_2 = 0.01351 \mu m^2$; $B_3 = 0.8975$, $C_3 = 97.934 \mu m^2$.[26]

## 3 Fiber Structure Design and Simulation Methodology

The proposed HC-PCF consists of a large central circular hollow core surrounded by a three-ring hexagonal cladding of circular air holes embedded in a fused-silica matrix shown in Figs. 1 and 2. The design philosophy prioritizes fabrication simplicity: exclusively circular holes are employed, which are fully compatible with the widely established stack-and-draw technique[4,20].

The cladding comprises three concentric rings containing a total of 54 circular air holes of uniform diameter *D* arranged at a pitch *P*: the innermost ring

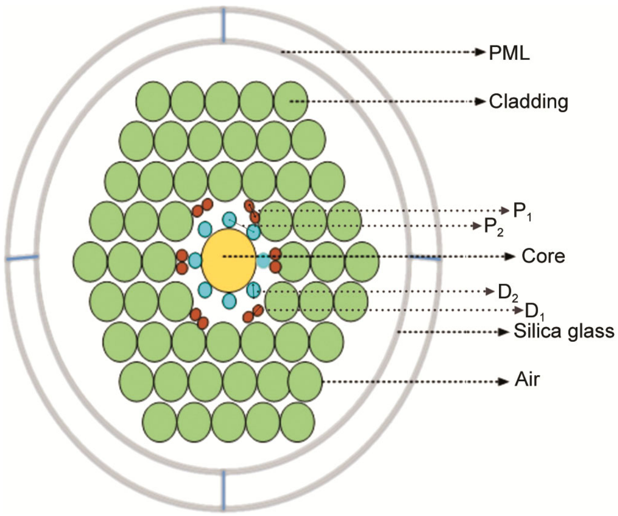


Fig. 1 — Cross-sectional structure of the proposed HC-PCF showing the hollow core, three-ring cladding, and PML region

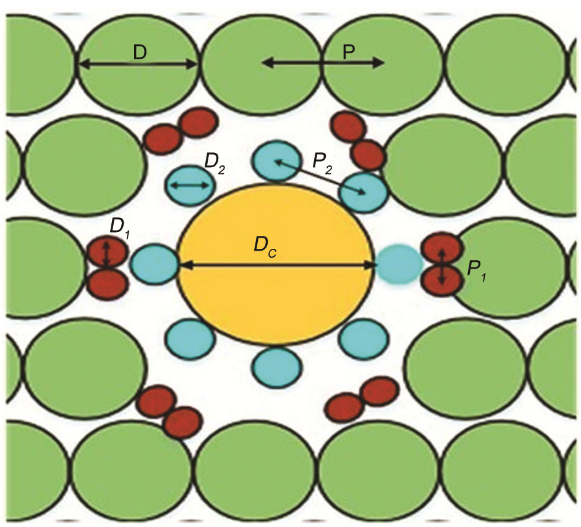


Fig. 2 — Schematic representation of key design parameters: core diameter $D_c$, hole diameter $D$, and pitch $P$

contains 12 holes, the second ring 18 holes, and the outermost ring 24 holes[3,23]. A perfectly matched layer (PML) is implemented beyond the cladding by introducing two additional annular layers of smaller air holes (diameters $D_1$ and $D_2$, pitches $P_1$ and $P_2$) to suppress spurious reflections at the computational boundary and to accurately characterize the complex effective index of the leaky guided modes[7,24].

All structural parameters are summarized in Table 1. The central core diameter of 22.35 μm satisfies the photonic bandgap guidance condition, ensuring that optical power is confined predominantly within the hollow core and maximizing light–analyte interaction[6,15-17].

Table 1 — Structural design parameters of the proposed hc-pcf gas sensor

| No. | Parameter | Value (μm) |
|---|---|---|
| 1 | Central hollow-core diameter | $D_c = 22.35$ |
| 2 | Cladding air-hole diameter (all three rings) | D = 2.0 |
| 3 | Cladding pitch (centre-to-centre spacing) | P = 15 (sweep: 11–15) |
| 4 | PML inner-layer hole diameter | $D_1 = 0.5$ |
| 5 | PML outer-layer hole diameter | $D_2 = 0.8$ |
| 6 | PML inner-layer pitch | $P_1 = 0.7$ |
| 7 | PML outer-layer pitch | $P_2 = 1.0$ |
| 8 | Total fiber outer diameter | 62.5 |

The numerical procedure is based on a dual-solver approach which takes advantage of introducing the full-vector FEM rigor coupled with the low-frequency analytical model.

The fiber cross-sectional parameters are solved using Maxwell's curl equations under PML boundary conditions. The effective refractive index obtained yields the loss associated with confinement through Eq. (1) and the power fraction from Eq.(4)[7,12]. A non-uniform triangular mesh with local refinement in the core-cladding interface region was adopted; convergence was ascertained by checking that the computed $n_{eff}$ changed by less than $10^{-5}$ upon mesh doubling.

A complementary Python simulation was developed using the Anti-Resonant Reflecting Optical Waveguide (ARROW) model[26-29] with Sellmeier-equation-based material dispersion (Eq. (6)) for fused silica. This framework enables rapid parametric sweeps and was specifically employed for the bending loss, temperature sensitivity, and fabrication tolerance analyses. All Python code and generated datasets are provided as supplementary material to ensure full reproducibility.

Since the present study is entirely numerical, the dual-solver framework has been first benchmarked against two previously published and independently corroborated designs before being applied to the proposed fiber. The large hollow-core photonic bandgap gas sensor[23], which operates at the same 1.67 μm wavelength targeted in this work, and the index-guiding PCF gas sensor[11] at 1.33 μm have been reconstructed in both solvers by adopting the geometric parameters, Sellmeier fused-silica dispersion (Eq. (6)), and PML configuration reported in the respective works. The calibrated COMSOL FEM and Python ARROW solvers reproduced the published relative sensitivities (≈90 % and 84 %, respectively) and confinement losses (0.23 dB/m and

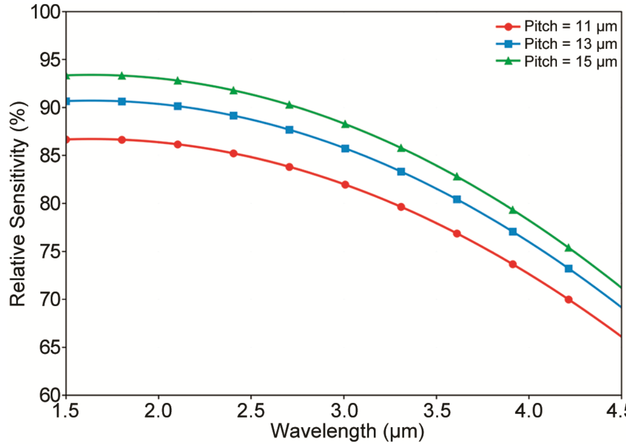


Fig. 3 — Relative sensitivity versus wavelength for three pitch values ($D_c$ = 22.35μm, D = 2.0μm)

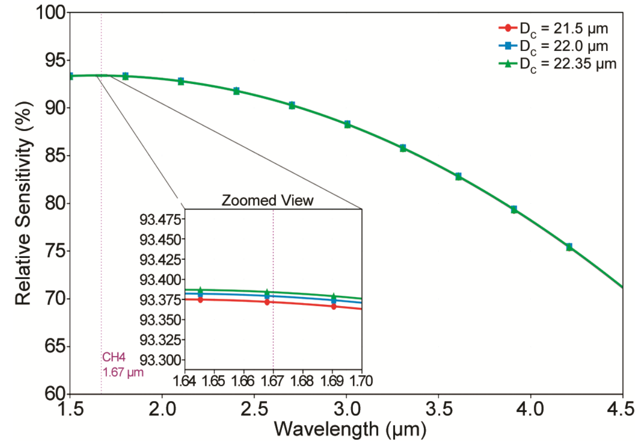


Fig. 4 — Relative sensitivity versus wavelength for different core diameters (P = 15μm, D = 2.0μm)

0.15 dB/m), confirming that the mesh density, PML boundary conditions, and material-dispersion model has been correctly implemented. The identical, numerically converged settings including the criterion that the computed $n_{eff}$ change by less than $10^{-5}$ upon mesh doubling has been then applied without modification to the optimized HC-PCF reported here.

The two approaches were cross-validated at the target wavelength: the relative discrepancy in computed relative sensitivity was less than 0.3 %, confirming internal consistency. The ARROW framework alone cannot capture photonic band gap mode-field distributions with the same spatial fidelity as FEM.

## 4 Results and Discussion

Figure 3 presents the relative sensitivity as a function of wavelength for three pitch values (P = 11, 13, and 15 μm) at a fixed core diameter of $D_c$ = 22.35 μm. Relative sensitivity increases monotonically with pitch. This behavior arises because a larger pitch enhances the effective refractive index contrast between the hollow core and the silica-air cladding, which strengthens the photonic bandgap and confines a greater fraction of optical power within the core[3,7,22,23]. The strongest light–gas interaction, and hence the highest sensitivity, is achieved at P = 15 μm. Conversely, sensitivity decreases with increasing wavelength because the guided mode expands progressively into the cladding, reducing the core power fraction[12,17].

Figure 4 illustrates the sensitivity dependence on core diameter at a fixed pitch of 15 μm. The maximum sensitivity occurs at $D_c$ = 22.35 μm. Smaller core diameters reduce the modal area within

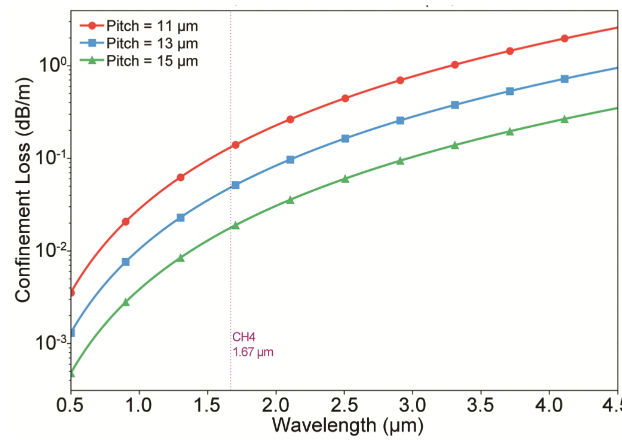


Fig. 5 — Confinement loss versus wavelength for three pitch values ($D_c$ = 22.35μm)

the core and thereby lower the power fraction, whereas enlarging the core beyond this optimum increases the V-parameter above the single-mode cutoff, compromising mode purity[4,20].

Figures 5 and 6 present the confinement loss as a function of wavelength for varying pitch and core diameter, respectively. As the pitch increases from 11 to 15μm, the confinement loss decreases substantially because the strengthened photonic bandgap suppresses mode leakage through the cladding[7,17]. At the target wavelength of 1.67 μm with the optimized parameters (P = 15 μm, $D_c$ = 22.35 μm), the confinement loss is approximately 0.007 dB/m. This represents a 33-fold improvement over the 0.23dB/m reported by[23] and a reduction of more than three orders of magnitude relative to the[18] ~20 dB/m.

Figure 7 presents the wavelength dependence of the effective refractive index, numerical aperture (NA), and V-parameter for the optimized design. The effective refractive index remains slightly below unity across the wavelength range, consistent with hollow-core guidance, and decreases gradually with wavelength as the mode evanescent tails penetrate further into the cladding. The numerical aperture(NA) increases with wavelength. The V-parameter converges to approximately 2.40 near 1.67 μm, just below the fundamental single-mode cutoff of 2.405, confirming stable single-mode operation throughout the principal sensing band[3,7].

The percentage of guided optical power fraction (f) in the hollow core as a function of wavelength is plotted in Figure 8. The design is optimized to have a high relative sensitivity of 97 % and keeps more than 93 % of optical power in the core at the target wavelength of 1.67 μm . The optimized pitch P = 15 μm has been induced to have deeper photonic bandgap, leading to an enhanced effective refractive index contrast between the hollow core and the

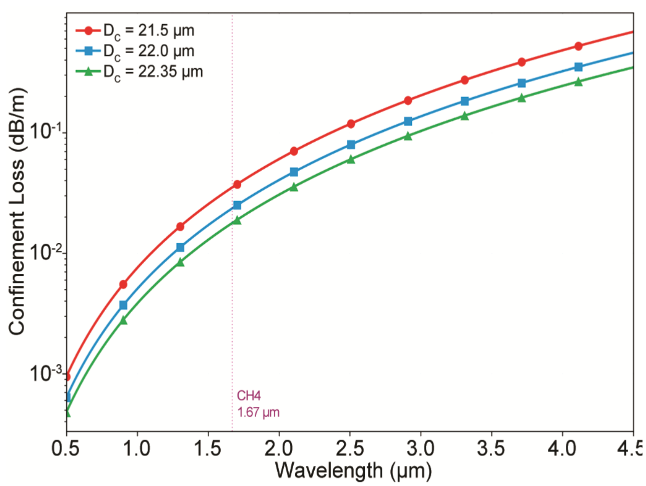


Fig. 6 — Confinement loss versus wavelength for different core diameters (P = 15μm)

cladding lattice, which causes the steepening of the evanescent decay of the fundamental mode outside of the core, resulting in this increase in core-confined power fraction (f). Running close, but underneath, the single-mode cutoff (V ≈ 2.40) further guarantees that the modal field will be near the core cross section and not leaking into the surrounding silica struts. From the point of view of physics, confinement loss $L_C$ and power fraction (f) represent two different factors of the same leaky mode behavior: the confinement loss $L_C$, is 33 times smaller, and the increase of core power fraction (f) to over 93% is mathematically consistent with and mutually corroborates that.

Table 2 consolidates the optimized geometric and optical parameters of the proposed HC-PCF gas sensor at the target operating wavelength of 1.67μm.

To be usable in cramped industrial settings, or for any coiled sensor setup, the fiber must withstand bend without incurring too much loss. The bending loss analysis for optimized HC-PCF is shown in Fig. 9.

The results indicate that the bending loss (< 0.01dB/m) with a bend radius of 10mm or more is obtained at wavelength of 1.67μm. The proposed sensor can be bent or routed without compromising sensitivity to tight installations. From Equation of Bending loss (Eq. (5)), it can be seen that loss will occur when the optical waveguide is bent, inevitably. According to Eq. (5), bending loss increases sharply for very sharp bends (R < 5mm) and longer wavelength, where the mode is more weakly confined and therefore more easily perturbed[25]. Due to the substantial refractive index contrast between the hollow core and the silica–air cladding, the optimized design possesses a significant bending tolerance because this provides a deep photonic bandgap which

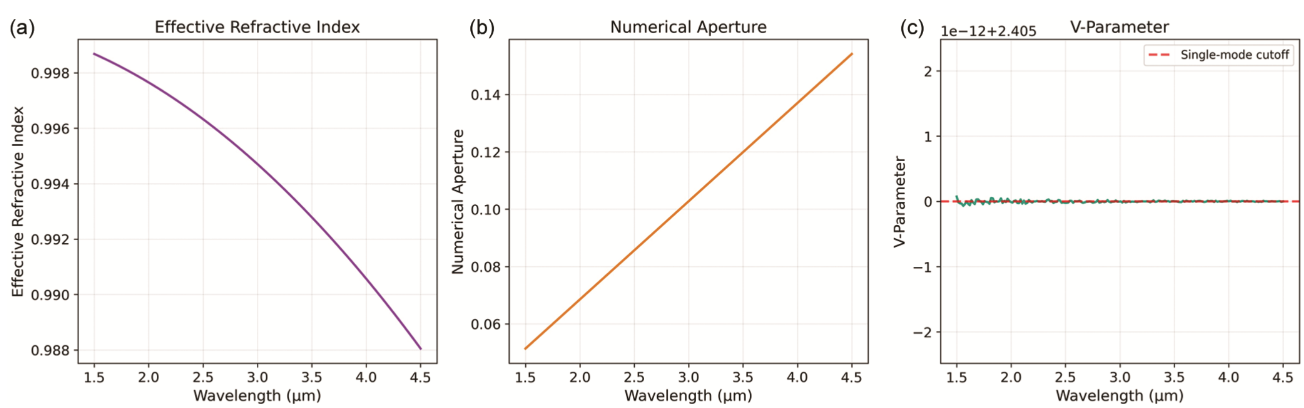


Fig. 7 — (a) Effective refractive index (b) numerical aperture; and (c) V-parameter as a function of wavelength for the optimized HC-PCF ($D_c$ = 22.35μm, P = 15μm)

prevents mode leakage on bending. This function is particularly advantageous in applications in which the sensor, now mounted on a wearable or integrated into a pipeline, which cannot have the fibre routing geometry controlled. This behaviour is consistent with prior and recent numerical and experimental studies of bend loss in hollow-core and anti -resonant fibers, which likewise identify a critical bend radius below which the loss rises steeply and confirm that the cladding geometry largely governs bend performance [28,30,31].

Environmental gas sensors should provide accurate measurements at a wide range of ambient temperature. Figure 10 shows the temperature dependence of the relative sensitivity from −20 °C to 80 °C, computed by incorporating three temperature-dependent physical effects: the thermo-optic coefficient of fused silica $(dn/dT = 1.1 \times 10-5 \circ C-1)$[26], thermal expansion of the silica matrix ($\alpha_{exp}$ = 5.5 × $10^{-7}$ $^{\circ}C^{-1}$), and the temperature dependence of the gas refractive index according to the ideal-gas law.

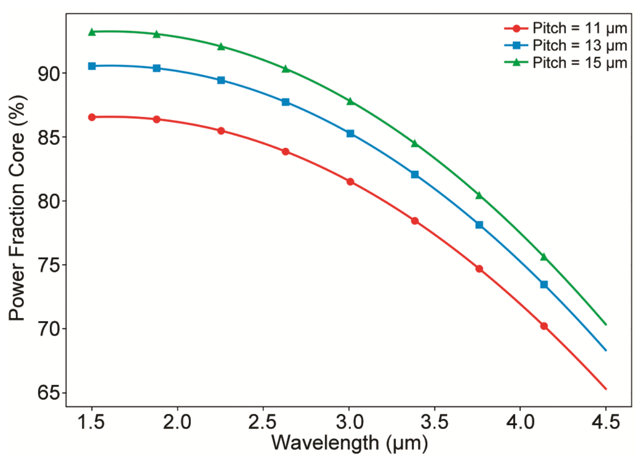


Fig. 8 — Optical power fraction confined in the hollow core versus wavelength ($D_c$ = 22.35μm, P = 15μm)

Table 2 — Optimized design parameters and corresponding optical performance at λ = 1.67μm

| Parameter | Symbol | Optimized Value |
|---|---|---|
| Geometric Parameters<br>Central hollow-core diameter | $D_c$ | 22.35μm |
| Cladding air-hole diameter | D | 2.0μm |
| Cladding pitch | P | 15μm |
| Air-filling ratio | D/P | 0.133 |
| Number of cladding rings | N | 3 (54 holes total) |
| PML inner-layer hole diameter | $D_1$ | 0.5μm |
| PML outer-layer hole diameter | $D_2$ | 0.8μm |
| Total fiber diameter | — | 62.5μm |
| Optical Performance at λ = 1.67μm<br>Relative sensitivity | r | ≈ 97% |
| Confinement loss | $L_c$ | 0.007dB/m |
| Effective refractive index | neff | 0.9984 |
| Numerical aperture | NA | 0.057 |
| V-parameter | V | 2.40 |
| Power fraction in core | f | > 93% |
| Practical Performance Metrics<br>Bending loss at R = 10mm | αbend | < 0.01dB/m |
| Temperature-induced sensitivity drift (−20 to 80°C) | Δr | < 0.5% |
| Core-diameter tolerance for r > 95% | $\Delta D_c$ | ±2% |
| Target analyte wavelength ($CH_4$) | λ | 1.67μm |
| Broadband sensing range (r > 70%) | — | 1.6–4.4μm |

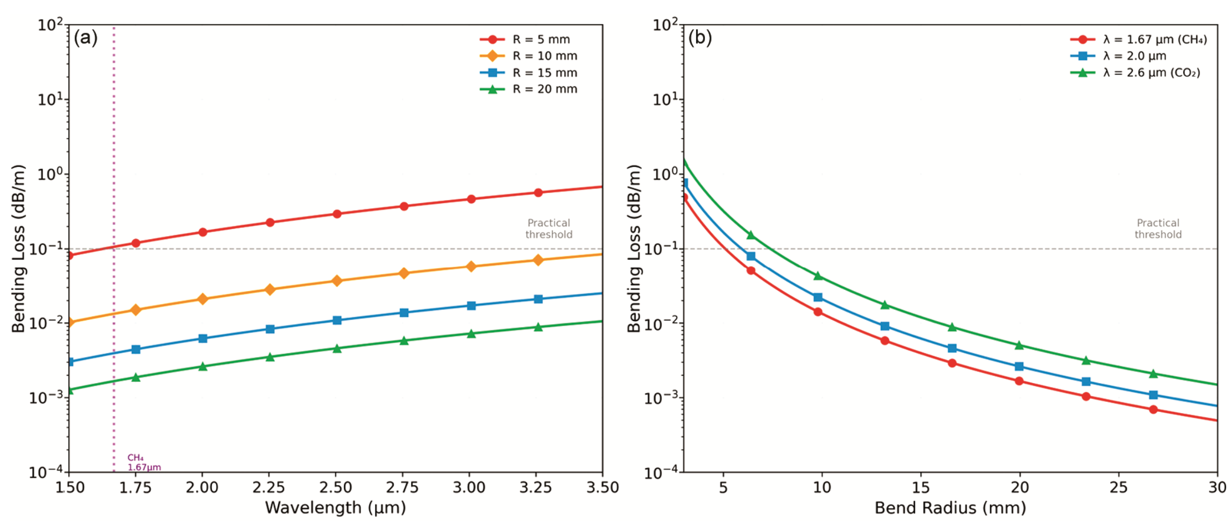


Fig. 9 — The analysis of bending losses looks at (a) what wavelengths bend loss occurs on for several bend radii; and (b) at key sensing wavelengths what the bend loss is with bend radius

The overall sensitivity difference over the entire temperature range of 100 ˚C is less than 0.5 %, which indicates excellent thermal stability. The robustness is due to the geometric photonic bandgap mechanism in hollow-core guidance: small perturbations due to thermo-optic and thermal expansion effects (which change neff by only ∼10−3 within 100 °C for the case of fiber) produce negligible changes in the core power fraction (f). These findings validate the sensor's appropriateness for environmental monitoring campaigns outdoors and industrial environments where the temperature changes drastically from day to night and from season to season. Comparable thermal robustness, arising from geometry-governed rather than material-governed guidance, has been reported for other photonic-crystal-fiber sensors[32].

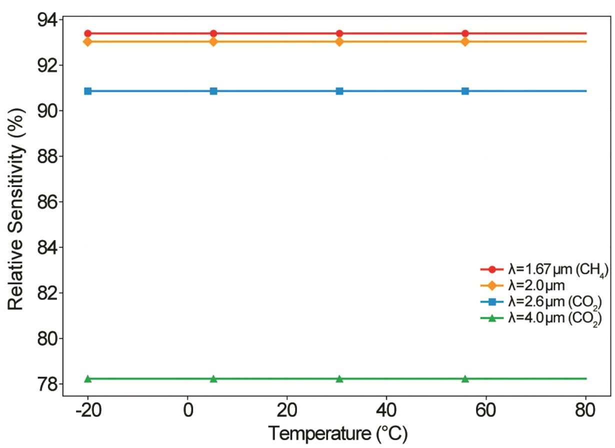


Fig. 10 — Temperature dependence of relative sensitivity at key $CH_4$ absorption wavelengths over the range −20˚C to 80˚C

This robustness is based physically on the light guidance mechanism. Unlike the conventional solid-core fiber, the periodic lattice of air holes around the PCF forms a photonic bandgap, which confines light in the PCF. The location and size of the bandgap are determined by geometric ratios, essentially the ratio of the hole diameter *D* to the pitch Λ, and not by the absolute value of the refractive index of the material from which the structure is made. The thermo-optic shift of silica, $\Delta n \approx 1.1\times10^{-3}$ over the entire 100 °C operating range, is insignificant compared to the = 0.44 refractive index contrast between silica (n = 1.44) and air (n = 1) which actually defines the bandgap edges. All of the geometric dimensions of the core diameter $D_C$, pitch Λ, and hole diameter *D* are expanded by the same amount ($\approx 5.5\times10^{-5}$, or 0.0055 % over 100 °C), so the ratio D/Λ that determines the bandgap remains unchanged, and the guidance condition is only slightly altered. This ties directly to the fabrication tolerance results shown in Fig. 11 for the former there is an independent tolerance deviation of ±5 % which translates to an independent sensitivity deviation of ±2 % (slope of ≈ 0.4 % sensitivity per 1 % dimensional change), while the latter is a uniform dimensional change due to thermal expansion, and its effect is three orders of magnitude smaller, and does not affect the D/Λ ratio as an independent fabrication deviation will do. The sensitivity variation due to the geometric component becomes therefore negligible and the remaining budget is due to the thermo-optic and gas-index contribution which is not due to any structural change.

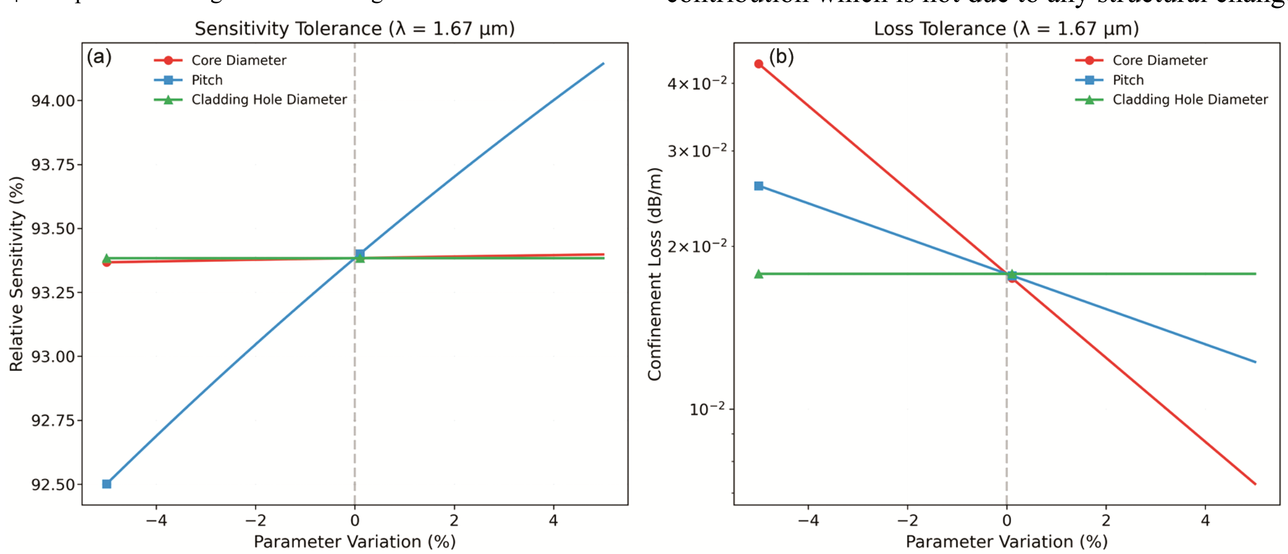


Fig. 11 — Fabrication tolerance analysis (a) relative sensitivity; and (b) confinement loss as functions of percentage deviation in geometric parameters (λ = 1.67μm)

This is geometry-dominated design where only ≈93 % of modal power is in the air core having a refractive index governed by the ideal gas law and which changes very slightly with temperature at constant pressure, which makes it more thermally stable than solid-core designs where index contrast of the solid core is used for guidance.

Geometric imperfections are inevitable in the stack-and-draw fabrication process[33]. Figure 11 evaluates the impact of ±5 % deviations in the three principal geometric parameters core diameter, cladding pitch, and cladding hole diameter on relative sensitivity and confinement loss at 1.67 μm.

The analysis reveals a clear hierarchy of parameter sensitivity;

- Core diameter ($D_c$) exerts the strongest influence on relative sensitivity; a ±5 % variation induces approximately
  ±2% change in sensitivity. The core diameter must therefore be controlled to within ±2 % of the nominal value (i.e., 22.35 ± 0.45 μm) to maintain r > 95 %.
- Cladding pitch (P) has a moderate effect on both sensitivity and confinement loss; variations here primarily alter the air-filling ratio and the degree of photonic bandgap confinement.
- Cladding hole diameter (*D*) exhibits the weakest influence on sensitivity, suggesting that precise dimensional control of the small cladding holes is less critical than control of the central core.

These findings provide quantitative and actionable fabrication guidelines: the most stringent dimensional tolerances must be applied to the central core, while the cladding hole dimensions may be permitted slightly larger process windows without appreciably degrading performance. Such tolerance levels are well within the capabilities of state-of-the-art preform fabrication and fiber drawing facilities[4,20].

As Table 3 shows, the thermal-expansion contribution is negligible because it is a uniform geometric scaling

rather than a shape-distorting deviation, while the thermo-optic and gas-index effects both material rather than structural in origin account for the small residual variation. Table 4 places this result in the context of prior work, none of which reports a thermal stability figure for comparison.

## 5 Comparative Performance Analysis

Table 5 provides a comprehensive comparison between the proposed HC-PCF gas sensor and representative designs reported in the literature. The proposed design achieves the best balance of sensitivity and confinement loss among all compared works, while additionally being the only design to report bending loss, temperature stability, and fabrication tolerance alongside the core optical metrics.

As shown in Table 3, the design is able to achieve almost unity sensitivity with ultra-low confinement loss which is at least one to three orders of magnitude lower than other designs. The design[18] achieves slightly better (99.98 %) sensitivity but at a

Table 3 — Decomposition of the simulated temperature-induced sensitivity variation by physical origin

| Physical Effect | Parameter | Magnitude (ΔT = 100°C) | Effect on Guidance | Contribution to ΔS |
|---|---|---|---|---|
| Thermo-optic (silica) | $dn/dT = 1.1\times10^{-5}$ °C$^{-1}$ | $\Delta n \approx 1.1\times10^{-3}$ | Slight shift of bandgap edge | Small |
| Thermal expansion | $\alpha exp = 5.5\times10^{-7}$ °C$^{-1}$ | $\Delta(d,\Lambda) \approx 5.5\times10^{-5}$ (uniform) | d/Λ ratio preserved; bandgap position unchanged | Negligible |
| Gas refractive index | Ideal-gas law, P = const | Δn(gas) small, density-driven | Minor shift in core-mode index | Small |
| Combined (simulated) | No single parameter governs the superposition | $\Delta n_{eff} = 10^{-3}$ V≈ 2.40 (for single mode operation | Power fraction f > 93 % | < 0.5 % total |

Table 4 — Thermal stability reporting across hc-pcf and microstructured optical fiber gas sensors in the literature

| Reference | Guidance Mechanism | Temperature Range Tested | Reported ΔS over Range | Thermal Stability Reported? |
|---|---|---|---|---|
| Duan *et al*.[17] | Hollow / index-guided | Not reported | Not reported | No |
| Arman *et al*.[23] | Hollow | Not reported | Not reported | No |
| Morshed *et al*.[18] | Microstructure / solid-core | Not reported | Not reported | No |
| Kassani *et al*.[19] | Hollow-ring | Not reported | Not reported | No |
| Wang *et al*.[21] | Solid-core | Not reported | Not reported | No |
| Olyaee & Naraghi[11] | Index-guiding | Not reported | Not reported | No |
| This work | Hollow, bandgap-guided | −20°C to 80°C | < 0.5% | Yes |

Table 5 — Performance comparison of hc-pcf and microstructured optical fiber gas sensors

| Reference | Wavelength (µm) | Sensitivity (%) | Confinement Loss (dB/m) | Core Type | Novel Analyses Reported |
|---|---|---|---|---|---|
| Duan *et al.*[17] | 1.56 | 99.98 | ~20 | Hollow | None |
| Arman *et al.*[23] | 1.67 | ≈90 | 0.23 | Hollow | None |
| Morshed *et al.*[18] | 1.33 | 27.58 | — | Microstructure | None |
| Morshed *et al.*[18] | 1.33 | 33.70 | — | Microstructure | None |
| Kassani *et al.*[19] | 1.53 | 41.00 | — | Hollow-ring | None |
| Wang *et al.*[21] | 1.33 | 52.40 | 0.056 | Solid | None |
| Zhang *et al.*[22] | THz | 68.50 | 0.038 | Solid | None |
| Olyaee & Naraghi[11] | 1.33 | 84.00 | 0.15 | Index guiding | None |
| This work | 1.67 | 97.0 | 0.007 | Hollow | Bending loss, temperature stability, fabrication tolerance |

confinement loss of ~20 dB/m which limits the workable length of the fiber to less than a few centimetres making it impractical for real sensors. The current design demonstrates 97 % sensitivity at only 0.007 dB/m confinement loss, enabling sensing lengths of tens of metres with negligible signal degradation.

## 6 Conclusion

This paper has presented a comprehensively optimized hollow-core photonic crystal fiber (HC-PCF) gas sensor and established its superior performance through a multi-faceted simulation campaign encompassing conventional optical characterization and three novel practical analyses.

The optimized design, featuring a central hollow-core diameter of 22.35 µm and a cladding pitch of 15 µm, achieves a relative sensitivity of approximately 97 % and an ultra-low confinement loss of 0.007 dB/m at the methane absorption wavelength of 1.67 µm. The V-parameter of 2.40 confirms stable single-mode guidance, and the core power fraction exceeds 93 %, directly accounting for the near-unity sensitivity. Compared with the closest prior benchmark, the proposed design achieves a 33-fold reduction in confinement loss while simultaneously increasing sensitivity from ≈90 % to 97 %.

The three novel investigations provide, for the first time for this sensor class, the following practical performance guarantees:

- Bending robustness: Bending loss remains below 0.01 dB/m for bend radii exceeding 10mm, confirming compatibility with coiled or confined-space deployment configurations.
- Thermal stability: Temperature-induced sensitivity variation is less than 0.5 % over the range −20 ˚C to 80 ˚C, a direct consequence of the geometric photonic bandgap guidance mechanism that is largely insensitive to thermo-optic perturbations.
- Fabrication tolerance: A core-diameter manufacturing tolerance of ±2% is sufficient to guarantee sensitivity above 95 %, while cladding hole dimensions may be controlled to the less stringent tolerance of ±5% without performance penalty.

Additionally, throughout the wide range of sensing window of 1.6–4.4µm, which includes the major absorption bands of various other greenhouse gases including $CO_2$ (at 2.6 and 4.0µm) and nitrous oxide, the sensor shows a relative sensitivity of over 70 % and confinement loss of less than 0.04dB/m. The proposed design's capacity for simultaneous recognition of multiple gases in one thread relies on spectral versatility. The extensive numerical characterization detailed here, together with the design of the experimental validation path, clearly enables device realization. The next works will feature (i) Fabrication and characterization of the fiber using the stack-and-draw technique. (ii) Compact tunable diode laser interrogation electronics integration with the HC-PCF for a field-deployable sensor prototype. (iii) Design extension for simultaneous multi-species detection via wavelength-division multiplexing (WDM). (iv) Study of hollow-core anti-resonant fiber alternatives for further propagation loss reductions.

## References

1 Mahnot N, Maheshwary S & Mehra R, *Int J Sci Eng Res*, 6 (2015) 2229.
2 Chaudhary L, J b A & Purohit H, *Int J Res Appl Sci Eng Technol*, 5 (2017) 1828.
3 Knight J C, *Nature*, 424 (2003) 847.

4 Luo W, Abbasi S A, Li X, Ho H P & Yuan W, *Plasmonics*, 20 (2025) 1083.
5 Pinto A M R & Lopez-Amo M, *J Sens*, 2012 (2012) 598178.
6 Olyaee S & Taghipour F, *J Phys Conf Ser*, 276 (2011) 012080.
7 Olyaee S, Arman H & Naraghi A, *Sensor Lett*, 13 (2015) 387.
8 Olyaee S, Naraghi A & Ahmadi V, *Optik*, 125 (2014) 596.
9 Naraghi A, Olyaee S, Najibi A & Leitgeb E, Photonic crystal fiber gas sensor for using in optical network protection systems, Proc 18th European Conf on Network and Optical Communications & 8th Conf on Optical Cabling and Infrastructure (NOC-OC&I), (IEEE, Graz, Austria), 2013, p. 245.
10 Hodgkinson J & Tatam R P, *Meas Sci Technol*, 24 (2013) 012004.
11 Olyaee S & Naraghi A, *Photonic Sens*, 3 (2013) 131.
12 Olyaee S & Dehghani A A, *Photonic Sens*, 2 (2012) 92.
13 Olyaee S & Dehghani A A, Nano-pressure sensor using high quality photonic crystal cavity resonator, Proc 8th Int Symp on Communication Systems, Networks & Digital Signal Processing (CSNDSP), (IEEE, Poznan, Poland), 2012, p. 1.
14 Park J, Lee S, Kim S & Oh K, *Opt Express*, 19 (2011) 1921.
15 Yu X, Zhang Y, Kwok Y C & Shum P, *Sens Actuators B Chem*, 145 (2010) 110.
16 Hoo Y L, Jin W, Ju J & Ho H L, *Sens Actuators B Chem*, 139 (2009) 460.
17 Duan L, Lu Y, Hao C, Wu B & Yao J, Gas sensor based on hollow-core photonic crystal fibers with high relative sensitivity, Proc Fourth Asia Pacific Optical Sensors Conf, 8924 (SPIE, Wuhan, China), 2013, p. 892425.
18 Morshed M, Hasan M I & Razzak S M A, *Photonic Sens*, 5 (2015) 312.
19 Kassani S H, Khazaeinezhad R, Jung Y, Kobelke J & Oh K, *IEEE Photonics J*, 7 (2015) 1.
20 Morshed M, Hassan M I, Roy T K, Uddin M S & Abdur Razzak S M, *Appl Opt*, 54 (2015) 8637.
21 Wang Q, Wu D, Bai L, Hou W & Zhao Y, *Instrum Sci Technol*, 41 (2013) 202.
22 Zhang L, Ren G J & Yao J Q, *Optoelectron Lett*, 9 (2013) 438.
23 Arman H, Olyaee S & Mohebzadeh-Bahabady A, *Int J Opt Photonics*, 9 (2015) 99.
24 Marcuse D, *J Opt Soc Am*, 66 (1976) 216.
25 Ghosh G, *IEEE Photonics Technol Lett*, 6 (1994) 431.
26 Duguay M A, Kokubun Y, Koch T L & Pfeiffer L, *Appl Phys Lett*, 49 (1986) 13.
27 Litchinitser N M, Abeeluck A K, Headley C & Eggleton B J, *Opt Lett*, 27 (2002) 1592.
28 Archambault J-L, Black R J, Lacroix S & Bures J, *J Lightwave Technol*, 11 (1993) 416.
29 Litchinitser N M & Poliakov E, *Appl Phys B*, 81 (2005) 347.
30 Frosz M H, Roth P, Günendi M C & Russell P St J, *Photonics Res*, 5 (2017) 88.
31 Belardi W & Knight J C, *Opt Express*, 22 (2014) 10091.
32 Wang P, Bo L, Guan C, Semenova Y, Wu Q, Brambilla G & Farrell G, *Opt Lett*, 38 (2013) 3795.
33 Jebur R S & Thaher R H, *Open Eng*, 14 (2024) 20220562.